Electrical properties of TiO_2/CO_3O_4 core/shell nanoparticles synthesized by sol-gel method

W. Iqbal[a,c,*], M. Mekki[b], W. Rehman[c], B. Shahzad[d], U. Anwar[e], S. Mahmood[f], Md. E. Talukder[g]

[a]*Department of Chemistry and Chemical Technologies, University of Calabria,87036 Rende, Cosenza, Italy*

[b]*Physical chemistry laboratory of mineral materials and their application, National center for research in materials sciences, technopark Borej Cedria, Soliman, Tunisia*

[c]*Department of Chemistry, Hazara University, Mansehra, Pakistan.*

[d]*Soochow Institute for Energy and Materials Innovations, College of Energy, Soochow University, Suzhou 215006, China*

[e]*Laboratory of Materials Science and Nanotechnology (LMNT), Department of Biomedical Sciences, University of Sassari, CR-INSTM, Viale San Pietro, 07100, Sassari, Italy*

[f]*Department of Zoology, University of Chakwal, Chakwal 48800, Pakistan*

[g]*Institute on membrane technology, (CNR-ITM), Via Pietro BUCCI, 87036, Rende, Cosenza, Italy*

TiO_2/Co_3O_4 core-shell nanoparticles were successfully synthesized by the sol-gel method in two steps: the first step is the sol-gel synthesis of Co_3O_4 nanoparticles, and the second step is the synthesis of TiO_2/Co_3O_4 nanoparticles by sol-gel method. The obtained Co_3O_4 and TiO_2/Co_3O_4 core-shell nanoparticles were investigated utilizing X-ray diffraction, scanning electron microscopy, Fourier transforms infrared spectroscopy, diffuse reflectance spectroscopy, and conductivity measurement. X-ray diffraction analysis showed the presence of both Co_3O_4 and TiO_2 phases in TiO_2/Co_3O_4 core-shell nanoparticles; co3o4 nanoparticles have a cubic shape, and TiO_2 nanoparticles have a tetragonal shape. SEM images of Co_3O_4 nanoparticles show most of the particles are smoothly distributed, having separate boundaries, and images of TiO_2/Co_3O_4 nanoparticles showed that with an increase in calcination temperature, the size of the core-shell nanoparticles also increases. FTIR spectrum of both confirms the synthesis of Co_3O_4 and TiO_2/Co_3O_4 nanomaterials. Diffuse reflectance spectroscopy exhibited the band gaps of TiO_2/Co_3O_4 core-shell nanoparticles decrease with the increase of the temperature. The conductivity of the TiO_2/Co_3O_4 core-shell nanomaterials increases with an increase in temperature and also with an increase in frequency.

(Received November 8, 2022; Accepted March 17, 2023

Keywords: Cobalt oxide, Core-shell nanoparticles, Calcination, Characterization, Electrical properties

1. Introduction

In the last decade, core/shell nanomaterials have obtained much attention due to their unique properties and numerous potential applications [1-3]. They typically reveal enhanced physiochemical properties for optics, electrochemistry, electronics, magnetism, mechanics, and catalysis [4, 5]. The core/shell nanomaterials of an inorganic semiconductor consist of an inner metal oxide generally covered by a shell of another metal oxide [6]. TiO_2 core and Co_3O_4 as a shell nanomaterial attract researchers due to tremendous applications, such as dye-sensitized solar cells (DSSCs) [7], optoelectronic devices [8], and photocatalysis [9].

* Corresponding author: waseem.iqbal@unical.it
https://doi.org/10.15251/DJNB.2023.181.403

TiO_2 nanomaterial has present interest due to its remarkable application in gas sensors, dye-sensitized solar cells (DSSCs), photovoltaics, etc. Furthermore, the optical and electrical properties of TiO_2 nanomaterial are very motivating. It is well known that the band gap value of anatase-TiO_2 (3.2eV) is higher than that of the rutile-TiO_2 (3.0 eV). Also, like TiO_2 nanomaterials, Co_3O_4 nanomaterials are extensively utilized in many applications such as gas sensors, battery cathodes, electrochromic, catalysis, magnetic materials, and heterogeneous catalytic materials. Different methods are utilized to synthesize TiO_2/Co_3O_4 core-shell nanomaterials for different applications [10-15].

In the present work, TiO_2/Co_3O_4 core-shell nanoparticles were synthesized by the sol-gel method in two steps and studied their electrical properties. The first step is the sol-gel synthesis of Co_3O_4 nanoparticles, and the second step synthesizes TiO_2/Co_3O_4 nanoparticles by the sol-gel method. The obtained material was characterized by X-ray diffraction (XRD), scanning electron microscopy (SEM), Fourier transforms infrared spectroscopy (FT-IR), diffuse reflectance spectroscopy (DRS), and conductivity to determine its electrical properties.

2. Experimental

The entire chemicals were purchased from sigma- Aldrich having a purity of 99.5%. Analytical-grade chemicals were utilized during this work. All the glassware utilized was washed thoroughly with the chromic mixture, then with tape water, and finally washed with deionized water and dried at 120 °C.

2.1. Synthesis of Co_3O_4 nanoparticle by sol-gel method

The synthesis of core/shell nanomaterials consists of two steps: the first step is the sol-gel synthesis of Co_3O_4 nanoparticles, and the second step is the synthesis of TiO_2/Co_3O_4 core-shell nanomaterials by the sol-gel method. For the synthesis of CO_3O_4 nanomaterials as precursors, 5.95g of Cobalt chloride hexahydrate ($CoCl_2.6H_2O$) dissolved in 100 ml distilled water and mixed with 30 ml methanol in this solution, and 2 M sodium hydroxide solution (NaOH) were utilized because an alkaline solution is necessary for the preparation of Co_3O_4 nanomaterials since normally divalent metal ion does not hydrolyze in acidic atmospheres. The mixture was vigorously stirred for two h and maintained at a temperature of up to 50 °C. Then 2 M NaOH solution was added dropwise in the precursor solution and maintained pH up to 10, and a light pink gel was formed. The resultant light pink colored gel was washed with deionized water and dried at 150 °C in the oven for 5 hours, and then the Co_3O_4 nanoparticles obtain.

2.2. Synthesis of TiO_2/Co_3O_4 core-shell nanoparticle

For the synthesis of Co_3O_4 coated TiO_2 nanoparticles, in burette (A), 5.95g of cobalt chloride Hexa hydrated ($CoCl_2.6H_2O$) dissolved in 50ml of distilled water and added 15 ml of methanol. In another burette (B), 2 M NaOH solutions were utilized to synthesize core/shell nanoparticles. Take 1g of TiO_2 nanoparticles in a 250 ml beaker on the hot plate. Then added, slowly, $CoCl_2.6H_2O$ solution from the burette (A) and NaOH from the burette (B) to the TiO_2 nanoparticles beaker. The pH of the solution was maintained up to 10-11 for the better size of core/shell nanoparticles. The mixture was vigorously stirred for two and obtained gel-like core/shell nanoparticles with light pink color. After washing through deionized water, the core/shell nanoparticles dried at 150 °C to remove solvents from core/shell nanoparticles. After drying the core/shell nanoparticles, obtained three samples from the yield. One sample was taken at 150 °C calcination and the second sample calcined at 450 °C for 4 hours, and the third sample calcined at 900 °C for 4 hours.

3. Results and discussions

The obtained powder was characterized by X-ray diffraction (XRD), scanning electron microscopy (SEM), and Fourier transform infrared spectroscopy (FT-IR) to determine the structure, shape, size, morphology, and functional group of the particles.

3.1. XRD analysis

The obtained XRD pattern for Co_3O_4 nanomaterial in Fig. 1 possesses no diffraction peak as evidence that the synthesized cobalt oxide NPs have amorphous nature.

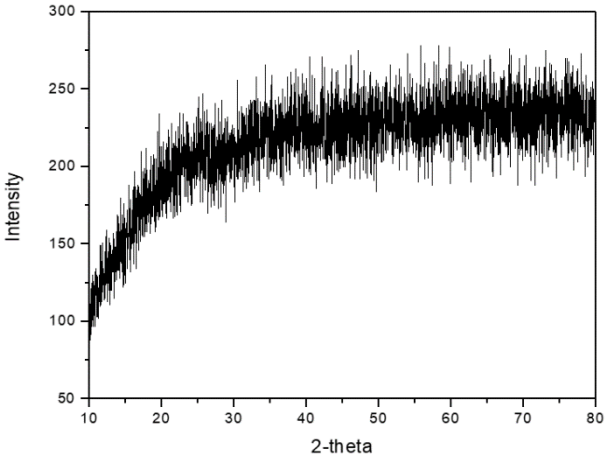

Fig. 1. XRD spectrum of cobalt oxide NPs.

The XRD spectrum given in Fig. 2 (a) represents Co_3O_4 coated TiO_2 calcined at 150°C possessing diffraction peaks at two theta positions with hkl values are 31.85(220), 36.48(311), 38.02(222), 54.99(422), 57.91(511), 65.11(440), 68.20(531), 69.40(442) and 78.82(622) matched with JCPDS no. 01-076-1802 corresponding to the cubic structure of Co_3O_4 NPs. While other peaks in the same spectrum (Fig. 2 (a)) at 26.71(110), 34.08(020), 47.79(210), 51.91(220), 56.54(221), 62.03(113), 63.05(310), 66.13(301) and 71.34(311) matched with reference card no. 01-076-0325 are attributed to TiO_2 with tetragonal geometry. The crystallite sizes calculated from XRD data using Debye-Scherer's equation for Co_3O_4 and TiO_2 are 40.65 and 34.98 nm, respectively. In fig. 2(b), the XRD patterns for Co_3O_4 coated TiO_2 calcined at 450 and 900°C possess characteristics peaks at 36.99(222) and 54.89(422) matched with peaks present in the JCPDS no. 01-076-1802, which confirm the cubic geometry of Co_3O_4 NPs. The diffraction peaks at 26.53(110), 34.08(020), 51.74(220), 63.56(310), 66.13(301), and 71.34(311) also matched with reference card no. 01-076-0325, which confirms the tetragonal shape TiO_2. Some peaks appeared in XRD spectra of the samples calcined at 450 and 900°C at 2 theta position with hkl values are 29.11(222), 35.97(331), 41.62(511), 45.74(440), 61.88(642), 64.60(731), 72.30(751) and 76.08(911) corresponding to JCPDS no. 01-075-0403. These peaks are assigned to the formation of cobalt titanium oxide with a chemical formula of Co_2OTiO_4 having a cubic geometrical shape. One peak with hkl value is 60.31(521) matched with reference card no. 00-029-0510 also due to the formation of cobalt titanium oxide with a chemical formula of $CoTiO_3$ having a cubic structure. The XRD study suggested that the Co_3O_4 and TiO_2 lead to the formation of cobalt titanium oxide at high temperatures. The diffraction peaks also become intense and narrow due to the increase in crystallite size. The crystallite sizes for cobalt titanium oxide from XRD data are 60.54 and 92.75 nm at 450 and 900°C respectively.

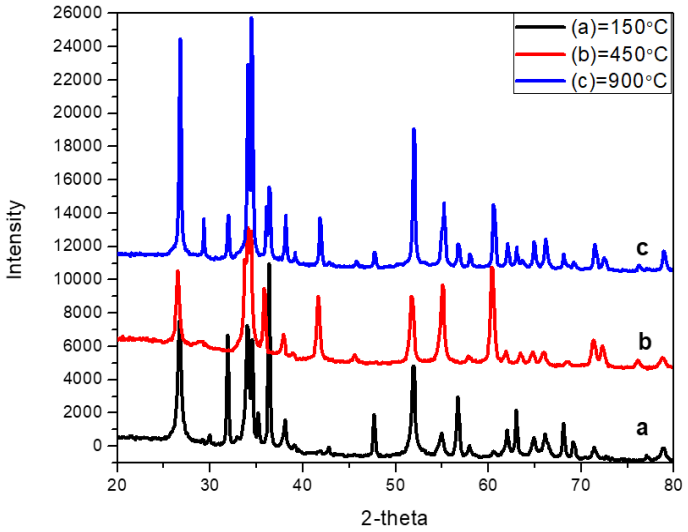

Fig. 2. XRD spectra Co_3O_4 coated TiO_2 calcined at 150, 450 and 900°C.

3.2. Scanning Electron Microscopy (SEM)

A highly magnified SEM image of cobalt oxide NPs gave as Fig. (a) shows that the majority of particles are smoothly distributed having separate boundaries however a bit of agglomeration was also seen. The SEM image given in Fig 3(b to d) represents the cobalt oxide coated TiO_2 calcined at 150, 450, and 900°C. The SEM micrograph of the sample calcined at 150°C shows that the particles are unevenly distributed and appeared in form of flexes. The agglomerated particles have no specific size or shape. However, upon increasing of calcination temperature the agglomerated particles appeared in the form of grains as shown in Fig 3(c), which represent the sample calcined at 450°C. The grains have distinct boundaries with irregular sizes and shapes. The SEM image of the sample calcined at 900°C given in Fig 3(d) shows a high degree of agglomeration.

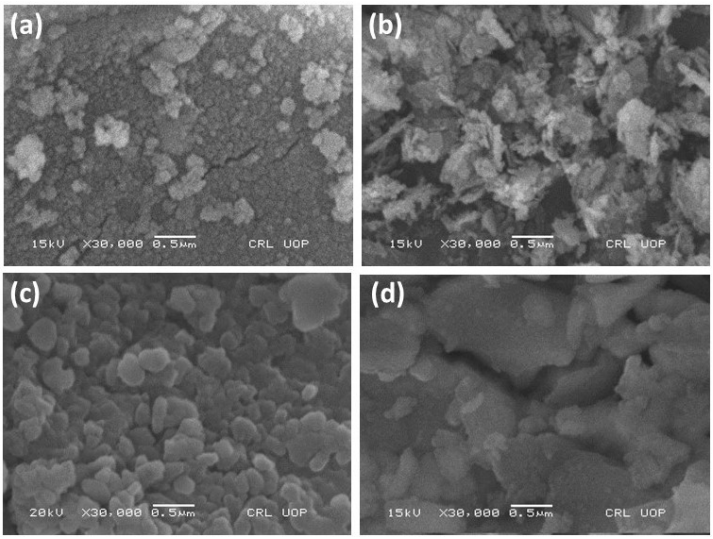

Fig. 3. SEM micrographs of cobalt oxide NPs (a) and cobalt oxide coated TiO_2 (b to d).

3.3. FTIR Spectroscopy

The FTIR spectrum of Co_3O_4 NPs possesses a broad band in the 3494-3298cm^{-1} area due to the water molecules. The band at 1415.41 cm^{-1} is assigned to $NO_3^{+2,}$ while the 1034.67 cm^{-1} is

due to C=C vibration. The bands at 1034.73 and 942.05 cm^{-1} are attributed to O-Co-O and Co-O-Co stretching vibration [16], while the bands 560.85 and 519.80 are due to the bending vibration of Co-O-Co and terminal Co-OH respectively [17]. The FTIR spectrum of Co_3O_4 coated TiO_2 calcined at 150°C exhibits a peak at 3586.12 and 1518.45 cm^{-1} due to the water molecules while 1230.25cm^{-1} O-Co-O vibration in the lattice. The bands at 663.90, 571.74, and 478.75cm^{-1} were assigned to Co-O-Co, Ti-O, and terminal Co-OH vibration [18]. The FTIR spectrum of Co_3O_4 coated TiO_2 calcined at 450°C possesses a band at 3359.92 cm^{-1} due to the stretching vibration of water molecules. The at 974.59 and 983.10 cm^{-1} in the spectra of both samples calcined at 450 and 900°C attributed to Co-O-Ti vibration, respectively. The peak gets intense with increasing calcination temperature suggesting the reaction between Co_3O_4 and TiO_2 [19]. Other peaks, 663.90 and 674.79 $cm^{-1,}$ are due to Co-O-Co, while the band at 560.85 and 571.75 cm^{-1} Ti-O.

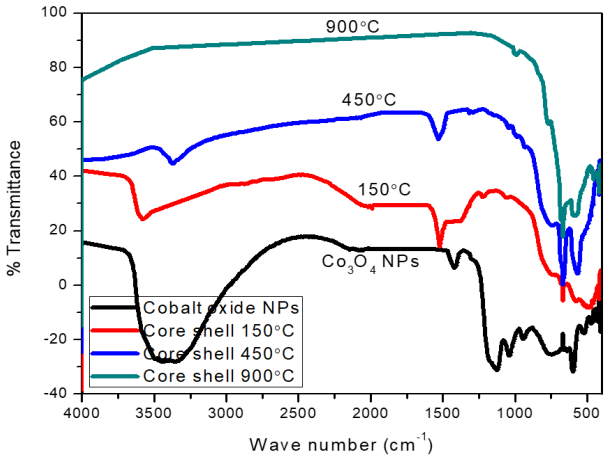

Fig. 4. FTIR spectra of cobalt oxide NPs and cobalt oxide coated TiO_2.

3.4. Diffuse Reflectance Spectroscopy

The optical properties of the core/shell nanoparticles are studied UV visible absorption spectroscopy (diffuse reflectance spectroscopy) Perkin Elmer UV_VIS/NIR spectrometer lambda 950 at NCP Islamabad, with integrating sphere of 200-2500 nm. The wavelength of the transmittance edge in UV-Vis spectra was determined by extrapolating the sharply rising part and the horizontal part of the UV-Vis curves shows the transmittance edge (as wavelength) according to previous findings [20]. The Absorbance edge was determined and the band gap energy was calculated on basis of the transmittance edge as shown in table 1. The band gap calculated for cobalt oxide NPs is 3.59 eV, higher than the previously reported values [22]. The clear difference in the band gap may be due to the amorphous nature of the synthesized cobalt oxide NPs. A red shift was observed in the DRS spectra of cobalt oxide coated TiO_2 with increasing calcination temperature, which resulted in a decrease in the band gap of the core/shell materials, as shown in table 3.1. This decrease in band gap energies with increasing heating temperature might be due to the increased energy of the electron of core/shell materials. Due to the reduction of carrier density caused by the removal of oxygen vacancies at high heating temperatures results in a decrease in band gap, which may be attributed to the Burstein-Mott shift [23].

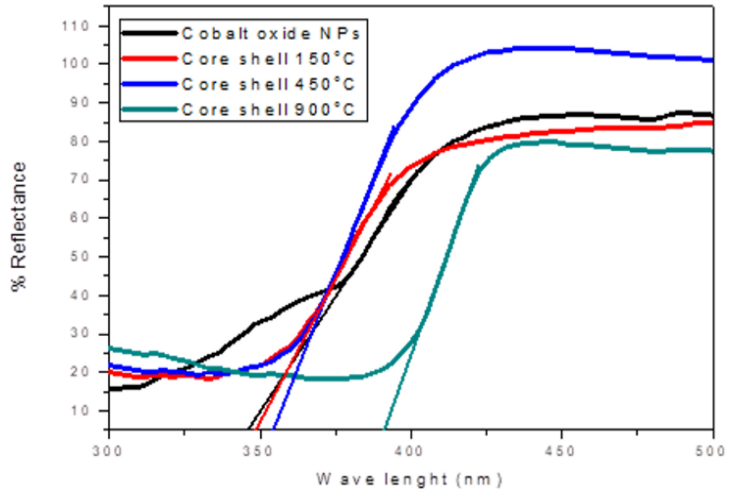

Fig. 5. DRS spectra of cobalt oxide NPs and cobalt oxide coated TiO_2.

Table 1. Absorbance edge and Band gap energy of cobalt oxide NPs and cobalt oxide coated TiO_2.

Parameters	Co_3O_4 NPs	Cobalt oxide coated TiO_2 calcined at different Temp (°C)		
		150	450	900
Absorbance edge (nm)	345.78	349.23	354.95	391.53
Band gap energy(eV)	3.59	3.56	3.50	3.18

3.5. Conductivity Analysis

The electrical conductivity spectra of the Co_3O_4-coated TiO_2 system calcined at different temperatures are shown in Fig. 6. The spectra possess two different regions, i.e. frequency independent region and a highly dispersive region. The low-frequency dispersion is due to the grain boundary while the high-frequency region is due to the conductivity of Co_3O_4-coated TiO_2 grains. This type of frequency-dependent behavior of semiconductor can be explained based on the double power law given as equation 1.1, which explains various factors that contribute to conductivity. Where the σdc is due the dc conductivity, $A_1\omega^{n1}$ related to low frequency dispersion (where $0 < n_1 < 1$) while $A_2\omega^{n2}$ explains high frequency dispersion region (where $0 < n^2 < 2$) [24].

$$\sigma_\tau(\omega) = \sigma_{dc} + A_1\omega^{n1} + A_2\omega^{n2} \qquad \text{Eq. 1.1}$$

The electrical charges get migrate under the influence of the applied electrical field to explore the conductivity behavior of the Co_3O_4-coated TiO_2 system. The spectra also show that the conductivity increases with the frequency and also with the calcination temperature. But it does not vary systematically with frequency, due to the randomness of the Co_3O_4-coated TiO_2 grains boundaries scattering and trapping of charge carriers [25].

The conduction is due to the exchange of electrons and holes between the same cation with different oxidation states present in the crystal structure. hopping probability of charge carriers depends upon the temperature, activation energy, and ions separation. In the Co3O4-coated TiO_2 system, the conduction may be due to the electron transmission between Co^{+3}-Co^{+4} and due to the hopping of holes among Ti^{+2}-Ti^{+3}. Thus, it is clear that the conduction arises due to the exchange of both electrons and holes between multi-oxidation states cations of Ti and Co

present in the cubic structure of the Co_3O_4-coated TiO_2 system [26]. However, the major contribution in conductivity is due to the electrons exchange interaction between Co^{+3}- Co^{+4} while a small contribution was also made by hole hopping among Ti^{+2}-Ti^{+3}. Thus, the concentration of Co cation plays a vital role in determining the electrical properties of the cobalt-titanium system.

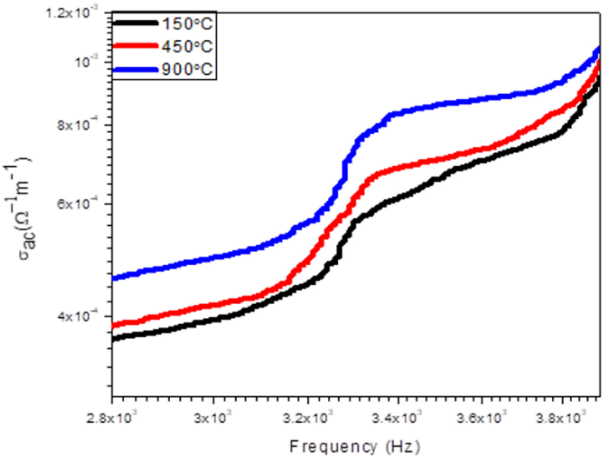

Fig. 6. Electrical conductivity of Co_3O_4 coated TiO_2 system.

4. Conclusion

The sol-gel method is adopted for the synthesis of the Co_3O_4 nanoparticles and TiO_2/Co_3O_4 core-shell nanoparticles. Scanning electron microscopy image showed that when the samples are calcined at 150, 450, and 900 °C the mean size of the Co_3O_4 coated TiO_2 was increased at 150, 450, and 900 °C showing that the calcination increased the average size of the Co_3O_4 coated TiO_2 due to the removal of the impurities. The TiO_2/Co_3O_4 core-shell nanoparticles present agglomerates and the shape of the particles are not well defined.

Co_3O_4 nanoparticles have cubically shaped; TiO_2 nanoparticles have tetragonal shaped. The crystallite sizes calculated from XRD data using Debye-Scherer's equation for Co_3O_4 and TiO_2 are 40.65 and 34.98nm respectively.

FTIR spectra confirm the formation of Co_3O_4 nanoparticles of also confirm the formation of TiO_2/Co_3O_4 core-shell nanoparticles. DRS spectra reveal that with the increase of temperature band gap decrease while with the decrease of temperature band gap increase. This trend shows that with an increase in temperature lowers the optical properties of synthesized core/shell nanoparticles. The reduction of carrier density caused by the removal of oxygen vacancies at high heating temperatures results in a decrease in the band gap, which may be attributed to the Burstein-Mott shift. The electrical conductivity increases with the calcination and increases with the increase in frequency.

References

[1] Mondal, K., & Sharma, A. (2016). RSC advances, 6(87), 83589-83612; https://doi.org/10.1039/C6RA18102C

[2] Bhattacharjee, Y., & Bose, S. (2021). ACS Applied Nano Materials, 4(2), 949-972; https://doi.org/10.1021/acsanm.1c00278

[3] Feng, H. P., Tang, L., Zeng, G. M., Zhou, Y., Deng, Y. C., Ren, X., ... & Yu, J. F. (2019). Advances in Colloid and Interface Science, 267, 26-46; https://doi.org/10.1016/j.cis.2019.03.001

[4] Joudeh, N., & Linke, D. (2022). Journal of Nanobiotechnology, 20(1), 1-29;

https://doi.org/10.1186/s12951-022-01477-8

[5] Noreen, S., Tahir, M. B., Hussain, A., Nawaz, T., Rehman, J. U., Dahshan, A., ... & Alrobei, H. (2021). International Journal of Hydrogen Energy.

[6] Maeda, K., Sakamoto, N., Ikeda, T., Ohtsuka, H., Xiong, A., Lu, D., ... & Domen, K. (2010). Chemistry-A European Journal, 16(26), 7750-7759; https://doi.org/10.1002/chem.201000616

[7] Murugadoss, G. (2022). Materials Research Foundations, 121.

[8] Luo, D., Li, X., Dumont, A., Yu, H., & Lu, Z. H. (2021). Advanced Materials, 33(30), 2006004; https://doi.org/10.1002/adma.202006004

[9] Singh, A., Ahmed, A., Sharma, A., Sharma, C., Paul, S., Khosla, A., ... & Arya, S. (2021). Physica B: Condensed Matter, 616, 413121; https://doi.org/10.1016/j.physb.2021.413121

[10] Fu, N., Jiang, X., Chen, D., Duan, Y., Zhang, G., Chang, M., ... & Lin, Y. (2019). Journal of Power Sources, 439, 227076; https://doi.org/10.1016/j.jpowsour.2019.227076

[11] Roy, A., Bhandari, S., Sundaram, S., & Mallick, T. K. (2021). Materials Chemistry and Physics, 272, 125036; https://doi.org/10.1016/j.matchemphys.2021.125036

[12] Semalti, P., & Sharma, S. N. (2020). Journal of nanoscience and nanotechnology, 20(6), 3647-3658; https://doi.org/10.1166/jnn.2020.17530

[13] Kazmi, S. A., Hameed, S., Ahmed, A. S., Arshad, M., & Azam, A. (2017). Journal of Alloys and Compounds, 691, 659-665; https://doi.org/10.1016/j.jallcom.2016.08.319

[14] Manikandan, V. S., Palai, A. K., Ramadoss, A., Mohanty, S., & Navaneethan, M. (2022). Materials in Electronics, 33(11), 8655-8664; https://doi.org/10.1007/s10854-021-06724-6

[15] Kawade, A. N., Bhujbal, P. K., Supekar, A. T., Sonawane, K. M., Pathan, H. M., Shaikh, S. F., & Al-Kaitani, A. A. (2021). ES Energy & Environment, 14, 73-78.

[16] Patil, V., Joshi, P., Chougule, M. and Sen, S., 2012. Soft Nanosci Lett, 2, pp.1-7; https://doi.org/10.4236/snl.2012.21001

[17] Salavati-Niasari, M., Khansari, A. and Davar, F., 2009. Inorganica Chimica Acta, 362(14), pp.4937-4942; https://doi.org/10.1016/j.ica.2009.07.023

[18] Salavati-Niasari, M., Khansari, A. and Davar, F., 2009. Inorganica Chimica Acta, 362(14), pp.4937-4942; https://doi.org/10.1016/j.ica.2009.07.023

[19] Usai, V., Mugadza, T., Chigondo, F., Shumba, M., Nharingo, T., Moyo, M., & Tshuma, P. (2019). Polyhedron, 157, 192-199; https://doi.org/10.1016/j.poly.2018.10.002

[20] Md. T. Uddin, Y. Nicolas, C. Olivier, T. Toupance, L. Servant, M. M. Müller, H. J. Kleebe, J. Ziegler, W. Jaegermann, Inorg. Chem. 2012, 51, 7764−7773; https://doi.org/10.1021/ic300794j

[21] Barakat, N.A., Khil, M.S., Sheikh, F.A. and Kim, H.Y., 2008. The Journal of Physical Chemistry C, 112(32), pp.12225-12233; https://doi.org/10.1021/jp8027353

[22] N. Nagarani, 2013. J. on Photo. and Spint: 2 2324 - 8572.

[23] N. Ortega, Ashok Kumar, P. Bhattacharya, S. B. Majumder, and R. S. Katiyar, Phys. Rev. B 77 (2008) 014111; https://doi.org/10.1103/PhysRevB.77.014111

[24] C. V. Ramana, Y. D. Kolekar, K. Kamala Bharathi, B. Sinha, and K. Ghosh, J. Appl. Phys.114 (2013) 183907; https://doi.org/10.1063/1.4827416

[25] M Younas, M Atif, M Nadeem, M Siddique, M Idrees and R Grossinger, J. Phys. D: Appl. Phys.44 (2011) 345402; https://doi.org/10.1088/0022-3727/44/34/345402

[26] Gao, P., Hua, X., Degirmenci, V., Rooney, D., Khraisheh, M., Pollard, R., ... & Rebrov, E. V. (2013). Journal of Magnetism and Magnetic Materials, 348, 44-50; https://doi.org/10.1016/j.jmmm.2013.07.060